Journal of Chromatography A, 1216 (2009) 6906–6916

Contents lists available at ScienceDirect

Journal of Chromatography A

journal homepage: www.elsevier.com/locate/chroma

Characterisation of porous materials for bioseparation

M. Barrande[a], I. Beurroies[a], R. Denoyel[a,*], I. Tatárová[b], M. Gramblička[b], M. Polakovič[b], M. Joehnck[c], M. Schulte[c]

[a] Universités d'Aix-Marseille I, II et III-CNRS, UMR 6264, Laboratoire Chimie Provence, Equipe Matdiv, Centre Saint Jérôme, F-13397 Marseille Cedex 20, France
[b] Department of Chemical and Biochemical Engineering, Institute of Chemical and Environmental Engineering, Faculty of Chemical and Food Technology, Slovak University of Technology, Radlinského 9, SK-812 37 Bratislava, Slovakia
[c] Performance & Life Science Chemicals R&D, Merck KGaA, Frankfurter Land Str. 250, 64293 Darmstadt, Germany

ARTICLE INFO

Article history:
Received 22 April 2009
Received in revised form 15 July 2009
Accepted 27 July 2009
Available online 26 August 2009

Keywords:
Size-exclusion
Mercury porosimetry
Gas adsorption
Thermoporometry
Vapour desorption

ABSTRACT

A set of chromatographic materials for bioseparation were characterised by various methods. Both commercial materials and new supports presenting various levels of rigidity were analysed. The methods included size-exclusion and capillary phenomena based techniques. Both batch exclusion and inverse size-exclusion chromatography were used. Gas adsorption, mercury porosimetry and thermoporometry were applied as well as a new method based on water desorption starting from the saturated state. When the rigidity of adsorbents is high enough, the agreement is reasonable between the values of the structural parameters that were determined (surface area, porosity, and pore size) by various methods. Nevertheless, a part of macroporosity may not be evidenced by inverse size-exclusion chromatography whereas it is visible by batch exclusion and the other methods. When the rigidity decreases, for example with soft swelling gels, where standard nitrogen adsorption or mercury porosimetry are no more reliable, two main situations are encountered: either the methods based on capillary phenomena (thermoporometry or water desorption) overestimate the pore size with an amplitude that depends on the method, or in some cases it is possible to distinguish water involved in the swelling of pore walls from that involved in pore filling by capillary condensation.

1. Introduction

The pore structure of chromatographic adsorbents has direct effects on efficiency in preparative bioseparations. The characterisation of porous materials is a field of intense research activity because of the difficulty to describe materials that are highly heterogeneous in pore size, pore shape or pore network organisation. Some methods like nitrogen adsorption–desorption or mercury intrusion–extrusion are more or less considered as standards and many models are available to derive pore size distributions or surface area from corresponding data [1,2]. These methods often give rise to hysteretic phenomena that can be used to give information on pore network organisation [3,4]. For example, Armatas and Pomonis [5] used Monte Carlo techniques to adjust a random network to fit nitrogen adsorption–desorption measurements on porous silica particles. With the generated network, tortuosity and connectivity were determined.

Gas adsorption is limited to pores with radii smaller than 100 nm, whereas mercury porosimetry gives access to a large range of pore size, i.e. from 3 nm to 400 μm. Unfortunately, these two methods are based on capillary phenomena which may induce stress on the walls of the material both during sample preparation (the sample must be preliminary outgassed for both experiments) and during experiments where cycles of adsorption/desorption (resp. intrusion/extrusion) create depressure (resp. overpressure) stress on the pore structure. Because many porous materials for bioseparation are soft gels, these two methods cannot be applied in a standard way since the porous structure may be different between the dry and wet state. This is generally due to the swelling of the walls.

Consequently, inverse size-exclusion chromatography (ISEC) [6] is more and more considered as the best method to characterize chromatographic supports because it is an in situ method mostly applicable at the same conditions as the separation process. Here, the pore size is deduced from the variation of the pore volume being unaccessible to a molecule of given size. The set of probe molecules, generally polymers, must not be adsorbed by the material. Advantages and drawbacks of this method were recently analysed by Yao and Lenhoff [7]. The main advantages are the conservation of sample integrity, the easiness to carry out experiments and the simple equipment. There are no drastic operating conditions (like high pressure, low temperature and drying conditions for gas adsorption or mercury porosimetry) and, as a consequence, less significant morphological changes occur because experimental conditions are

* Corresponding author. Tel.: +33 491637127; fax: +33 491637111.
E-mail address: renaud.denoyel@univ-provence.fr (R. Denoyel).

0021-9673/$ – see front matter © 2009 Elsevier B.V. All rights reserved.
doi:10.1016/j.chroma.2009.07.075

similar to those of normal operations, which is especially important for swellable gels because their structure is greatly affected by the liquid content. It is also possible to observe the influence of salt concentration on pore size distribution [8].

The experimental drawbacks of ISEC are the duration of experiment, because the flow rate of the mobile phase in the column must be low enough to ensure equilibrium, and eventually the need of long columns for attaining appreciable resolution among different sized probes. Thus compression of the packed bed in the column may occur which could be a problem for soft materials. Nevertheless, the main difficulties are probably at the level of the interpretation of data and of the derivation of quantitative information on pore structure. Discrepancies may be observed when pore information derived from dextrans is applied to proteins, which is not surprising considering the appreciable property differences between these two classes of molecules [7].

Appropriate solvents relevant to practical use should be chosen, with additional considerations such as to minimize adsorption effects and favour optimal solute conformations. The total pore volume and interstitial space are typically measured by solute at opposite ends of the size spectrum of the standards. Considering the rigidity of the solutes, wall effects can affect precise evaluation of the exact values, with the significance depending on the relative abundance of pores. Dextran radii are calculated as if dextrans were hard spheres but in fact they are flexible and may penetrate pores smaller than their nominal size. Data are generally presented as partition coefficient (K) versus probe size. Partition coefficients do not reflect only the actual pore size but the interaction between the molecules and the walls too. Hubbuch et al. [8] showed the influence of salt concentration on ISEC data for an agarose grafted with dextran before coupling with sulfopropyl groups. At a low ionic strength, ISEC measurements show a low pore accessibility, because there are strong interactions between unshielded sulfopropyl groups. These might lead to a rather stiff network conformation which is difficult to penetrate for large molecules. At high ionic strength, the charges on sulfopropyl groups might be shielded and an increase in pore accessibility is observed. Finally, size-exclusion principle can be applied also in a batch mode where it is easier to get the equilibrium partition coefficient [9–11].

Like in other methods, the derivation of a pore size distribution from ISEC data is model dependent. A pore shape must be assumed and it must be kept in mind that usually only up to 15 points can be experimentally obtained, which can limit the detailed description of the pore size distribution. In the case of rigid samples, for example like silica monoliths, a good agreement is obtained with other techniques in the mesopore range (2–50 nm) whereas some differences may be observed in the macropore range, i.e. above 50 nm [12]. Recently, modelling methods of pore structure considering their connectivity based on ISEC data were developed [13,14].

Because it is always difficult to get reliable information from a single technique, it is useful to compare the results of ISEC with other techniques when possible. In this paper, comparisons will be made between the methods quoted above but also with two methods that are less common. The first one is thermoporometry [15], which is another method based on capillary phenomenology. Here the influence of confinement on melting/solidification of a fluid is studied. Thermoporometry has the advantage that a sample can be used in its application medium without drying step (only washing with a pure solvent). Its disadvantages are mainly due to the fact that melting–solidification in confined medium is less well understood than capillary condensation despite clear similarities [16]. Notably, the parameters used in the calculation models are not directly measurable, which means that a calibration needs to be done [15]. This method has often been proposed as a useful method for characterising soft materials, gels [17] or polymers [18].

Finally, the last method used for comparison is the liquid desorption method recently developed by Denoyel et al. [19], which is based on the determination of the desorption isotherm of a liquid from a porous medium starting in an excess of liquid. Pore size distributions are derived from capillary condensation theory like in the gas adsorption method. Because the various phenomena involved in these methods are of different nature, the comparison between the methods needs to choose a number of parameters that can be derived from all methods. Porosities and pore sizes will be compared. The determination of pore size or pore size distribution is a rather complex problem in any method because it needs a number of assumptions concerning pore shape and pore structure. This point will be discussed in detail for each method in Section 2 where thermoporometry and liquid desorption will receive more attention.

2. Materials and methods

2.1. Chromatographic stationary phases

Three ion exchange materials, one hydrophobic charge induction material, four protein A based affinity materials and four non-functionalized supports were analysed. The origin and the main initial characteristics of these materials are given in Tables 1 and 2.

2.2. Gas adsorption

When possible, nitrogen adsorption measurements were performed with a Micrometrics ASAP 2010 apparatus. Adsorption samples were first evacuated at a pressure lower than 10^{-3} Pa. The BET equation was applied to determine the surface area and the pore size distribution was calculated from the desorption branch

Table 1
Selected materials: origin and chemical composition.

Materials	Type and ligands	Supplier	Support
SP Sepharose Fast Flow	SO_3 ion exchange	Amersham Bioscience	Cross-linked agarose
Fractogel SE Hicap	SO_3 ion exchange	Merck	Cross-linked polyacrilic
S Ceramic HyperD F	SO_3 ion exchange	Ciphergen	Silica based ceramic
MEP HyperCEL	Hydrophobic Charge Induction Chromatography (HCIC) Sorbent: 4-mercapto-ethyl-pyridine	Ciphergen	Cross-linked cellulose
Mabselect	Protein A based affinity media	Amersham Bioscience	Cross-linked agarose
r ProteinA Sepharose FF	Protein A based affinity media	Amersham Bioscience	Cross-linked agarose
Poros 50A High Cap	Protein A based affinity media	PerSeptive	Polystyrene/divinylbenzene
Prosep vA High Cap	Protein A based affinity media	Millipore	Controled Pore Glass
Fractosil	Support	Merck	Silica
Fractogel	Support	Merck	Cross-linked polyacrylic
FractAIMs	Support	Merck	Cross-linked polyacrylic
Fractoprep	Support	Merck	Vinylic polymer

Table 2
Main physical properties of materials. Wall densities are determined by pycnometry with water.

Material	Typical size range of particles (μm[a])	Settled bed density of dried particles (g cm^{-3})	Particles wall density (g cm^{-3})
SP Sepharose Fast Flow	90	0.11	1.63
Fractogel SE Hicap	40–90	0.16	1.34
S Ceramic HyperD F	50	0.56	2.2
MEP HyperCEL	80–100	0.17	1.5
Mabselect	40–130		1.
r ProteinA Sepharose FF	105		1.5
Poros 50 A High Cap	50		1.1 (ref)
Prosep vA High Cap	75–150		2.5 (ref)
Fractosil	40–100		2.2
Fractogel	40–90		1.44
FractAIMs	75		1.3
Fractoprep	80		1.7

[a] As given by the manufacturers.

of equilibrium isotherm by the BJH method, whose principle is reminded in the paragraph about water desorption.

2.3. Mercury porosimetry

Mercury intrusion–extrusion measurements were carried out using a Micrometrics Autopore II 9220 mercury porosimeter. Samples were evacuated at room temperature and at least two intrusion–extrusion cycles were carried out for all samples. A contact angle of 130° was used to calculate the pore size distribution by the Washburn equation.

2.4. Thermoporometry

This method of characterisation of mesoporous solids is based on the monitoring of the melting and solidification of a confined fluid by means of differential scanning calorimetry (DSC) [15]. There is a relationship between the pore size and the temperature shift of the solid/liquid phase transition. For most systems, the melting/freezing temperature in pores is lower than in the bulk. The heat dissipated at a given temperature is proportional to the amount of phase-changing component. This means that the size and temperature location of the DSC peaks observed during the melting or the solidification of the confined fluid are directly related to the pore width distribution. The basic equation used in thermoporometry (and which is analogous to the Kelvin equation for capillary condensation) is

$$\frac{1}{R_p - t} = -\frac{1}{2\gamma_{sl}} \int_{T^\circ}^{T} \frac{\Delta_m H}{v_l T}\, dT \quad (1)$$

where R_p is the pore radius in which the solidification occurs at temperature T (T° is the bulk solidification temperature), γ_{sl} is the solid–liquid surface tension (here ice–water), $\Delta_m H$ is the melting enthalpy, v_l is the molar volume of the fluid and t is the thickness of the bound layer (assumed to be constant). This bound layer corresponds to a film of water between solid water and the pore wall that does not change phase in the considered temperature range. The existence of this layer is related to the conditions of surface melting that lead to a decrease of melting–solidification temperature as compared with the bulk one. The pore size distribution is derived directly from the DSC recording of the calorimetric peak by the following equation [15]:

$$\frac{dV}{dR_p} = k\frac{(\Delta T)^2}{Q} y \quad (2)$$

where y is the heat flow measured by the DSC and k is a constant that is related to the scanning rate of temperature and to the parameters of the equations $R_p = f(T)$ which are derived from Eq. (1). In the case of water, the following equations hold for cylindrical pore shape [15]:

$$R_p = \frac{-64.7}{T - T^\circ} + 0.5 \quad \text{in nm for solidification} \quad (3)$$

$$R_p = \frac{-32.3}{T - T^\circ} + 0.68 \quad \text{in nm for melting} \quad (4)$$

Before the experiment, the sample was washed three times with water. Around 50 mg of wet sample was then introduced in the DSC cell (a Setaram DSC 92 apparatus was used). The following temperature programme (Fig. 1) was selected after several calibrations tests on known rigid macroporous samples: (a) fast cooling at −20 °C to freeze water in the whole sample, (b) heating until −5 °C at 1 °C/min when melting in pores smaller than 15 nm occurs, (c) heating until −0.15 °C at 0.02 °C/min with melting in pores ranging between 15 and 300 nm, (d) cooling until −5 °C at 0.02 °C/min with solidification in the same pore range as in (d), and (e) heating

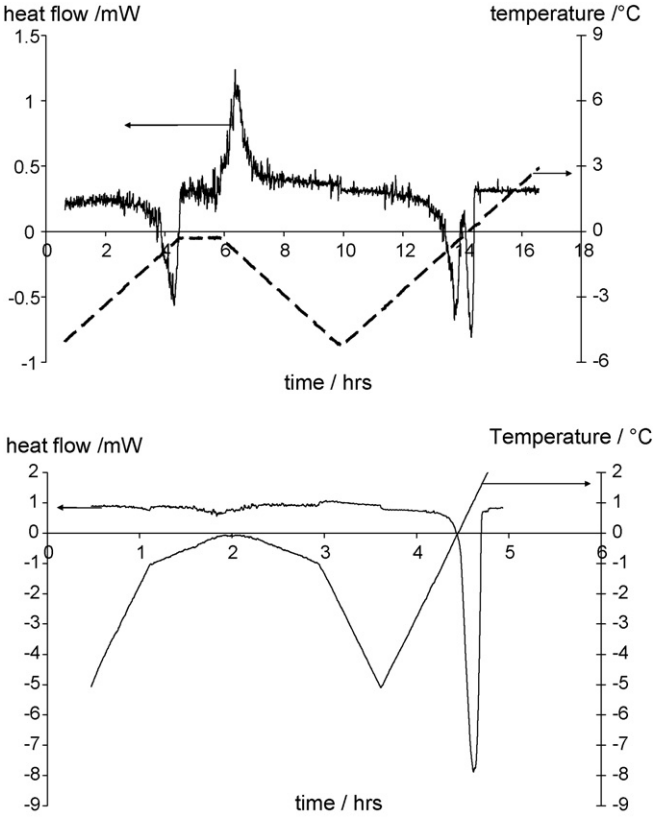

Fig. 1. Heat flow and temperature programme of thermoporometry experiments in the case of SPFF (top) and MEP HyperCEL (bottom).

until 5 °C at 0.02 °C/min with melting both in pores and bulk. Fig. 1 shows recordings of heat flow and temperature versus time for two samples: SP Sepharose Fast Flow (SPFF) and MEP HyperCEL. In the case of SPFF (Fig. 1a), melting and freezing of confined water are observable during the first cycle: they correspond to the first two peaks between 0 and 10 h where temperature stays below −0.15 °C. The two last peaks on the right-hand side of the plot correspond to melting of confined and bulk water, respectively when the sample temperature was raised above its bulk melting temperature. They are not completely separated but they clearly evidenced the contribution of each type of liquid. In that case, both melting and freezing peaks can be used to calculate pore size distributions by using Eqs. (3) and (4). In the case of MEP HyperCEL, the behaviour is totally different. No peak is observable during the first melting–freezing cycle and when the temperature of the sample is raised above 0 °C, only one peak is observed. It is not possible to separate here confined water from free water. This point will be discussed in Sections 3 and 4.

2.5. Water desorption

Water is evaporated from a sample saturated with water at a very low rate in order to get a quasi-equilibrium desorption isotherm of water. The procedure, which is detailed in a previous paper [19], consists in evaporating simultaneously the water which is in the two cells of a Tian Cavet type microcalorimeter: one with the sample immersed in water and the other with pure water. Vacuum is slowly created in the two cells through capillaries. Absolute pressure over the sample, differential pressure between the sample and the reference and heat flow are recorded versus time. The mass desorbed is calculated from the heat flow assuming desorption heat equal to vapourisation heat, which is a good approximation until the last two adsorbed layers. At the end of the experiment the sample is weighed. Knowing the initial mass of water in the cell, it is possible to plot the desorption isotherm. The desorption isotherm is then obtained from the mass desorbed versus relative pressure. Using a differential transducer, relative pressure very close to 1 can be measured.

The pore size distribution is calculated by the BJH method [20], which uses the Kelvin equation:

$$\ln \frac{P}{P^\circ} = -\frac{2\gamma.v_l}{r_K \cdot RT} \quad (5)$$

where P is the equilibrium pressure, P° is the saturation pressure, γ is the surface tension of the adsorbate (0.072 mJ m^{-2} for water) and v_l is its molar volume (18 cm^3 mol^{-1}). At each equilibrium pressure the volume of liquid desorbed corresponds to the emptying of pores until the radius r_K given by the Kelvin equation and to the decrease of the adsorbed layer in the pores that are already emptied. An iterative procedure is used to carry out the calculation. The thickness of the adsorbed layer is calculated by the Halsey equation that is based on disjunction pressure theory [21]:

$$t = \frac{k}{(\ln(P/P^\circ))^{1/3}}$$

where the constant k was determined by fitting the adsorption isotherm of water on a non-porous silica. The radius of a pore which is emptied at a given pressure is given by

$$r_p = r_K + t\left(\frac{P}{P^\circ}\right)$$

This approach is adapted to sufficiently rigid porous systems. Other models should be used for systems de-swelling during desorption. Nevertheless, it is always possible to derive a pore volume. The validity of the method was assessed for porous silica that was also studied by mercury porosimetry [19]. Because the surface tension of water is much smaller than that of mercury, it is possible to get data with samples that are too weak to resist to mercury pressure (let us remind that in a capillary filled by a wetting liquid, the walls must resist to a negative pressure). By starting with an excess of water, the desorption isotherm is determined from a relative pressure of 1 to a value close to 0. Since the pressure is accurately determined near $P/P^\circ = 1$ and the temperature of the sample is carefully controlled, it is possible to extend pore size determinations to a much larger range of pore sizes than those usually derived from nitrogen adsorption–desorption isotherm at low temperature. Nevertheless, the stress induced by water on the pore walls during desorption may be relatively high leading to deformation of the pore structure. Moreover, when the material walls are swelled by water, the de-swelling during drying will contribute to the desorption curve. Consequently the relationship between pore size, amount desorbed and equilibrium pressure will not obey the Kelvin equation. The water desorption experiment allows to determine the water content of the sample versus water activity. Each time the water environment changes, steps appear on the desorption curve. These steps can be used to determine various volumes (inter- or intraparticle pore volume, swelling volume) depending on interpretation. The pore size obtained from the Kelvin equation will be reliable only if the capillary effect is dominating the process of desorption. An example of desorption curve is given in Fig. 2 for sample Poros 50A with interpretation of the various domains.

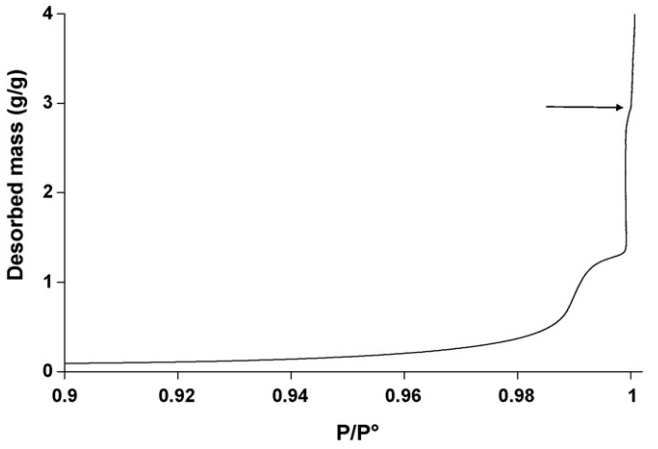

Fig. 2. Desorption isotherm of water from Poros 50A. The arrow indicates the beginning of interparticle desorption.

For the calculations of pore size by the Kelvin equation, it is assumed that the contact angle is zero. It is not always possible to check this value. In the case of rigid samples some experiments with another solvent having a different surface tension gave the same results. For swelling systems, it is not really possible to verify by the same method, but one may assume that swelling itself is a criterion of good affinity and wetting by water.

2.6. Size-exclusion methods

Both batch and chromatographic size-exclusion experiments were described in detail in a recent study [11] so only principal aspects of both methods are described in this section.

A set of saccharide and polysaccharide molecules differing in their weight-averaged molecular weights M_w from 180 for glucose to 22 500 000 for a dextran were used as solute probes [11]. Calculation of the hydrodynamic radius of the probes, r_s, was based on the Mark–Houwink–Sakurada equation [22,23]:

$$r_s = 0.027 M_w^{0.5} \quad (6)$$

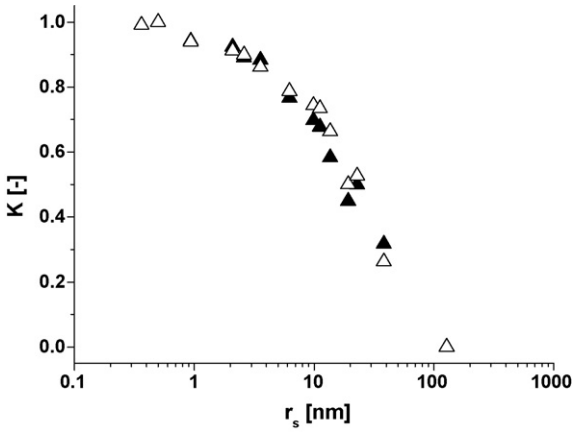

Fig. 3. Comparison of the accessibility curves obtained for the chromatographic material Mabselect by the batch (▲) and the chromatographic size-exclusion technique (△).

In the case of the three supports (FractoAIMS, Fractogel and Fractoprep) another set of polymers provided by PSS (Polymer Standard Services, Mainz) was used to perform ISEC experiments: these are dextrans and pullulans with M_w ranging between 180 and 16 700 000 g mol^{-1}. Viscosity radii provided by PSS were used in the calculation.

It was found in the previous paper [11] for a set of seven adsorbents from Table 1 that the batch and chromatography size-exclusion techniques provided comparable values of partition coefficients K, normalized between the values of 0 and 1 for the largest and smallest probes (Fig. 3). Moreover, chromatographic data had, in general, somewhat better reproducibility. No reliable values of accessible volumes could however be obtained directly from ISEC experiments for any adsorbent listed in Table 1. All size-exclusion data presented were made in triplicates.

2.7. Batch

Exact amounts of adsorbent particles with pores filled with a solvent (20 mM phosphate buffer, 100 mM NaCl, pH 7.2) were put into flasks containing predefined volumes of the probe solutions V_r. The flasks were sealed and stirred until equilibrium between the phases was reached.

The specific volume of pores accessible to a solute v_d was calculated from the following equation:

$$v_d = \left(\frac{c_m^0}{c_m^{eq}} - 1\right)\frac{V_r}{m_{ad}} \tag{7}$$

where c_m^0 and c_m^{eq} are the initial and equilibrium concentrations of a solute molecule, respectively, and m_{ad} is the mass of dry adsorbent. The total specific pore volume of adsorbent particles v_p was obtained from the water content obtained by drying wet particles at 60 °C. The specific pore volumes accessible to glucose and largest dextran, $v_{d,\min}$ and $v_{d,\max}$, respectively, were used to distribute the total specific volume of pores v_p among small, medium, and large pores. The fraction of the pore volume inaccessible to glucose molecules (hydrodynamic radius of 0.36 nm), $v_p - v_{d,\min}$, was assigned to small pores. The void volume accessible to the largest solute molecules (hydrodynamic radius of 124 nm), $v_{d,\max}$, was defined as the specific volume of large pores. The remaining pore volume fraction, which was partly accessible to individual solute probes, represented the volume of medium pores. Compared with the usual IUPAC classification, small pores (radius smaller than <0.36 nm) correspond to the beginning of the micropore range (pores smaller than 2 nm), medium pores covers the largest micropores, the mesopore range and the beginning of the macropore range; large pores are within the macropore range. Medium pores are the most significant for the separation of monoclonal antibodies. Large pores govern the rate of transport of separated molecules to the active sites of adsorbents. Small pores have a negligible contribution to the separation effect of adsorbents although they form a significant part of the specific surface area of pores.

2.8. Chromatography

Adsorbent particles were packed either into Pharmacia HR 5/5 (Amersham Biosciences AB, Uppsala, Sweden) or Superformance 150/16 (Gotec Labortechnik, Ramstadt, Germany) chromatographic columns using slurry-packing procedures recommended by suppliers. The columns were then equilibrated with a mobile phase (20 mM phosphate buffer, 100 mM NaCl, pH 7.2) and probe samples were injected.

The solute retention volume V_R was calculated from the first absolute moment of the distribution function obtained from the chromatographic signal. The V_R values were used to calculate the specific pore volumes accessible to individual solutes in the following way:

$$v_d = v_{d,\max} + \frac{V_R - V_{R,\max}}{V_{R,\min} - V_{R,\max}}(v_{d,\min} - v_{d,\max}) \tag{8}$$

where $V_{R,\min}$ and $V_{R,\max}$ are the retention volumes of glucose and the largest dextran and $v_{d,\min}$ and $v_{d,\max}$ are provided by batch experiments. The partition coefficients of the solutes were calculated from the equation,

$$K = \frac{V_R - V_{R,\max}}{V_{R,\min} - V_{R,\max}} \tag{9}$$

They were used to calculate the specific surface area s using the Giddings random plane model [24]:

$$K = \exp(-sr_s) \tag{10}$$

2.9. Calculation of volumetric pore size distribution

The volumetric fraction v_m of a pore of radius r accessible to a molecule of radius r_s is

$$v_m = \left(1 - \frac{r_s}{r}\right)^2 \tag{11}$$

If $f(r)$ is the pore size distribution function, $f(r)dr$ corresponds to the pore volume in the range between r and $r+dr$. For each probe of radius r_s, $f(r)$ is linked to v_d by the following relationship:

$$v_d = \int_{r_m}^{\infty} f(r)\left(1 - \frac{r_s}{r}\right)^2 dr \tag{12}$$

By using an Excell software procedure, this equation is inverted in order to get $f(r)$ ($f(r)dr$ values for each solute probe can be evaluated by fitting the experimental values of v_d with the model Eq. (12)). The pore size distribution obtained assumes only the pore shape but not distribution shape.

Pore size distributions were also calculated using the log normal distribution function:

$$f(r) = \frac{1}{\sigma r\sqrt{2\pi}} \exp\left[-\frac{1}{2}\left(\frac{\log(r/r_p)}{\sigma}\right)\right] \tag{13}$$

where σ is the dispersion of the distribution and r_p is the mean pore radius.

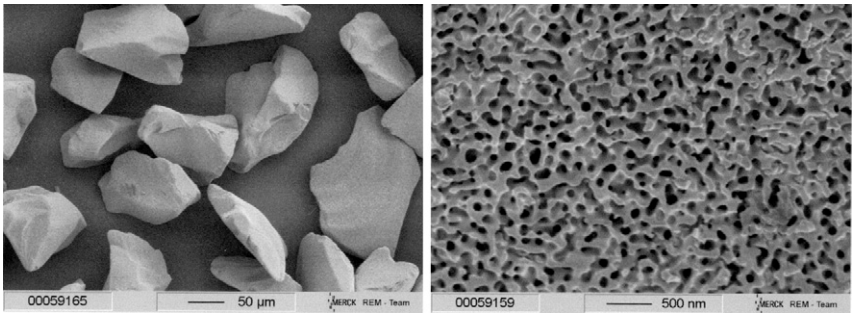

Fig. 4. SEM images of Prosep.

3. Results and discussion

The main parameters obtained by the various methods that were compared are surface area, pore size and porosities. Each of these parameters may be measured by several characterisation methods. The surface area of a material may be calculated from BET equation applied to gas adsorption but also from all the other methods provided a pore size distribution is obtained. All the methods indeed assume a pore shape when a pore size calculation is carried out; the surface area is then evalated from the surface volume ratio defined by this shape. The mean pore radius may be obtained by six methods: gas adsorption (applying BJH equation), water desorption (applying BJH equation), mercury porosimetry, thermoporometry and the two size-exclusion techniques.

The intraparticle volume (and then intraparticle porosity) is theoretically obtainable by the six methods but gas adsorption is not adapted to intraparticle pores if they are larger than 100 nm. Total pore volumes (intra + interparticle volume) are measurable only by three methods: mercury porosimetry, water desorption and water content by drying of wet particles (see the paragraph "Batch" in Section 2). It is noteworthy that the compression of the particle bed may be different for the various techniques. Finally, the density of the walls may be obtained either by mercury porosimetry or directly by pycnometry. In the following text, the results are classified as a function of the mechanical properties of the material. The results for rigid porous solids are presented first because they may be studied by all the methods using classical interpretations. Soft materials analysis will be presented and discussed in a second step. Prosep, Poros 50A and Fractosil were the rigid materials of interest in the following.

3.1. Rigid materials

The comparison of methods is first done for Prosep, that allows all the methods to be applied, including those creating a high stress

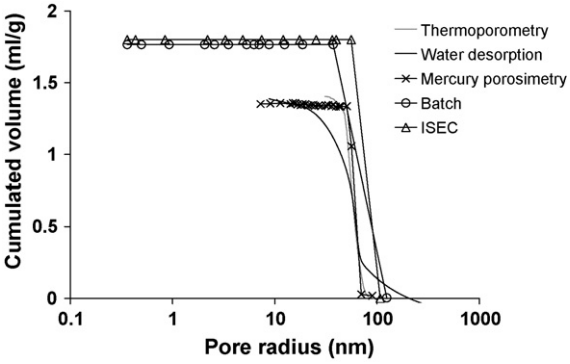

Fig. 5. Pore size distributions of sample Prosep obtained by various experimental methods.

on the structure (like mercury porosimetry). This material, based on controlled pore glass, is made of non-spherical irregular particles whose size is in the range 50–100 µm. The pore network is highly complex as shown in Fig. 4 but is made of regular pores as confirmed by the narrow pore size distributions obtained from different methods presented in Fig. 5 for the pore range below 10 µm (intraparticle pores). Mean pore size, interparticle volume, intraparticle volume, surface areas are given in Tables 3 and 4. There is a relatively good agreement between the various pore size distributions. Gas adsorption results are not given in Fig. 5, because this sample is macroporous and the nitrogen adsorption–desorption isotherm is reversible without any saturation plateau indicating the filling of pores. For such materials with large pores, mercury porosimetry is well suited. Both inter- and intraparticle pores may be evidenced. In Fig. 6, intrusion–extrusion curves for two cycles show reproducible hysteresis indicating that pores are not destroyed by mercury and mercury is not retained inside pores. In Fig. 7, the heat flow versus time recording of the thermoporometry experiment shows a good

Table 3
Specific pore volumes of materials.

Material	Pore volumes by size-exclusion (mL/g)				Pore volumes by mercury porosimetry (mL/g)		Pores volumes by water desorption (mL/g)		Pore volumes by thermoporometry (mL/g)
	Intra	Small pores	Medium pores	Large pores	Total	Intra	Total	Intra	Intra
SP Sepharose Fast Flow	6.05	1.80	3.27	0.99			9.0	5.9	2.9
Fractogel SE Hicap	3.85	0.61	2.20	1.04			5.9	3.6	
S Ceramic HyperD F							1.6	0.8	
MEP HyperCEL	5.78	0.31	3.83	1.64			10.6	5.7	
Mabselect	9.15	1.31	5.26	2.58			12	6.7	2.1
r ProteinA Sepharose FF	18.8	0.55	13.03	5.22			13.5	7.3	
Poros 50 A High Cap	1.58	0.47	0.43	0.68	4.2	2.3	3.0	1.4	1.3
Prosep vA High Cap	1.84	0.00	1.84	0.00	3.2	1.4	3.5	1.4	1.4
Fractosil					1.6	0.6	1.6	0.6	0.6
Fractogel					0.8	0.2	6.3	2.9	1.0
FractAIMs					3.3	0.6	7.8	4.7	1.1
Fractoprep					3.3	1.3	3.5	2.1	1.4

Table 4
Pore size and specific surface area of materials by various methods.

Material	Pore size by SE nm		Surface area RPM (m^2/mL)	BET Surface area ($m^2\ g^{-1}$)	Pore size by mercury porosimetry (nm)	Surface area by mercury ($m^2\ g^{-1}$)	Pores size by Water desorption (nm)	Surface area by Water desorption (nm)	Pore size by thermoporometry (freezing) (nm)
	CPM	LogNormal			Intra		intra	Intra	Intra
SP Sepharose Fast Flow	19.4	20.5	127				245	78	
Fractogel SE Hicap	21.7	24.1	115				32	163	
S Ceramic HyperD F							19	64	
MEP HyperCEL	23.7	23.8	101				127	163	
Mabselect	54.9	58.8	45.2				217	86	
r ProteinA Sepharose FF	52.4	53.8	49.8				265	79	
Poros 50 A High Cap	86	90.5	29.9	30		575	92	87	47
Prosep vA High Cap	89.4	95.8	26.7	26		51	62	51	55
Fractosil				21	28	45	30	37	24
Fractogel		53		22		65	25	189	33
FractAIMs		46		181	30	180	29	144	30
Fractoprep		38		197	7	214	10	340	30

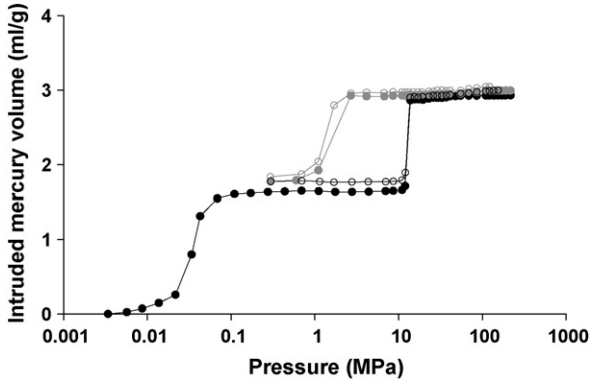

Fig. 6. Mercury porosimetry of Prosep—first cycle (closed circles) and second cycle (open circles).

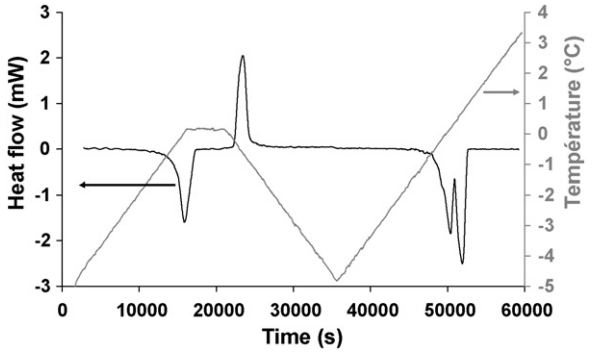

Fig. 7. Heat flow and temperature programme of thermoporometry experiment in the case of Prosep.

separation of melting peaks corresponding to inside and outside water. This indicates that thermoporometry may be used to characterize pore sizes in a larger range than the one accessible by gas adsorption analysis.

The values of the parameters for the three rigid samples are given in Table 4. The values are in agreement in many cases but some differences may be observed. For example, the intraparticle pore volume obtained for Fractosil by nitrogen adsorption is much smaller than by other methods. In spite of the hysteresis of the adsorption–desorption isotherm (Fig. 8), the saturation plateau is not well defined on the adsorption branch. It is however well defined on the desorption branch but corresponds to scanning inside the hysteresis. This problem is overcame in the water des-

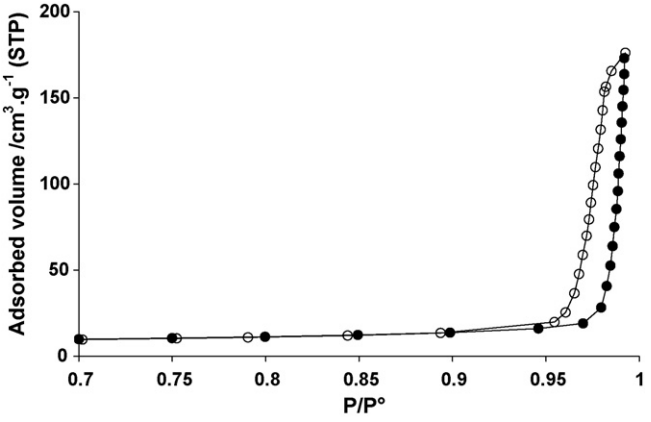

Fig. 8. Nitrogen adsorption (closed circles) desorption (open circles) onto Fractosil at 77 K in the high relative pressure range.

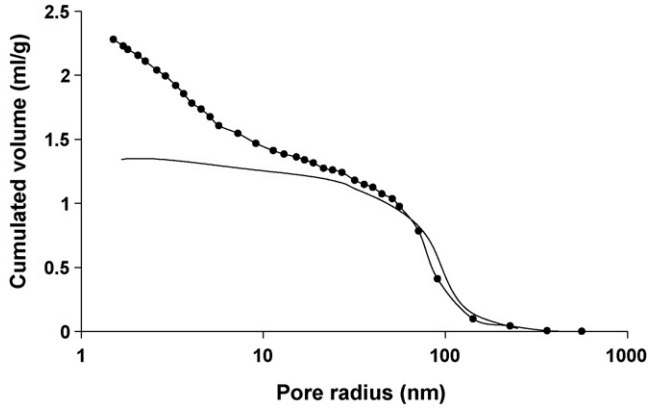

Fig. 9. Cumulative pore size distributions obtained for Poros 50A by mercury porosimetry (circles) and water desorption (continuous line).

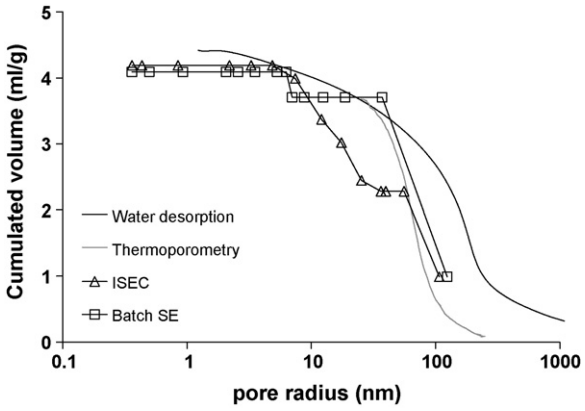

Fig. 11. Pore size distribution of Sepharose SPFF obtained by various methods.

orption method that starts from saturation and may measure very large pores, including interparticle pores. The total pore volumes are in agreement between the three adapted methods (mercury, water desorption and batch size-exclusion) except for Poros 50A, which shows a nonnegligible compressibility under mercury pressure conditions. This compressibility is documented in Fig. 9, which shows that mercury cumulated volume diverges from that of water desorption for pores smaller than 10 nm (which corresponds to intrusion pressures higher than 180 MPa).

3.2. Soft gel materials

Let us start the discussion by comparing results for Sepharose SPFF, which is a swelling gel made of agarose. The material has a form of highly porous spherical particles which are shown in the SEM picture of Fig. 10. Some of these particles are made of hollow spheres that contain themselves smaller spherical particles. At the scale of the image, the surface looks relatively smooth with pore entrances smaller than 1 μm, but one must keep in mind that the drying process probably modifies the pore size. Such swelling sample cannot be characterised by gas adsorption or mercury porosimetry because of de-swelling of the structure during the drying step. Only water desorption, thermoporometry and size-exclusion results are presented here.

In the case of water desorption, the experiments start from wet state and water is evaporated during a quasi-equilibrium procedure. Because a capillary stress is applied to the sample the resulting desorption isotherm corresponds both to pore emptying and de-swelling, but the contribution of each phenomenon to the measured water loss is unknown. The results of pore size distribution have to be considered as an equivalent pore size distribution where radii are determined by the Kelvin equation. In the case of thermoporometry, this sample gives rise to peaks of melting and solidification that are clearly different from those of the bulk (Fig. 1). This is not always the case with soft gels as was observed for other materials used in this study.

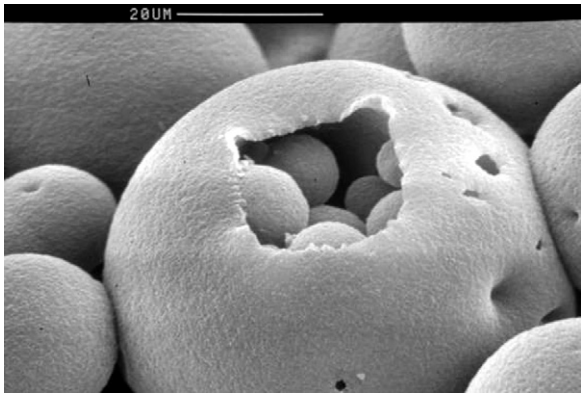

Fig. 10. SEM image of Sepharose SPFF.

The obtained pore size distributions are given in Fig. 11. Total pore volumes are in a reasonable agreement but the pore size distributions are really very different. The water desorption method leads to apparently very large pores and there is clearly a need to develop models that take into account the swelling behaviour of the sample. Nevertheless, this method is able to give values of the total pore volume and of interparticle pore volume (Table 4). In the case of thermoporometry the situation is also unclear. A shift of pore sizes towards higher value is expected from the discussion above. This is clearly evidenced by comparing with ISEC results that leads here to a mean pore radius of 10 nm against 65 nm and 160 nm, for thermoporometry and water desorption, respectively. ISEC seems to be the most reliable method for such sample since it is really an in situ method. Nevertheless, the comparison with batch size-exclusion indicates that the description of the sample in term of pore size is not simple. As seen in Table 3 there is a strong exclusion of the smallest probe (small pores volume) and a large fraction of pores inside particles with radii larger than 100 nm (large pores volume). Such large pores are evidenced by SEM images (notably pores between small particles that are inside the main particles, see Fig. 10). They also contribute to the desorption curve of water, but their quantitative determination, in size or volume, is not possible by any of the methods presented here.

This discussion about SPFF sample can be extended to the other soft materials. Data are summarized in Table 3. For most samples, the smallest probe is partially excluded from the pores whereas the largest one is not totally excluded from the particles. These two phenomena may be well quantified by the analysis of batch size-exclusion results. In Table 3, the various volumes defined in "experimental" part are reported. Among the analysed materials, only Prosep (rigid sample analysed in the first part) present both small pores and large pore contributions close to 0. All other samples, notably soft gels, have both contributions. The large contribution of micropores is not expected for such samples. It may correspond to the fact that swelling of the polymeric material by the solvent creates small pores not accessible to the smallest probe. The size of these pores that correspond to solvation of the chains of the polymeric material could be as small as one or two water molecular diameters. All samples made of soft gel contain macropores whose pore size determination is not possible by size-exclusion techniques. Moreover, these results show that the macropore contribution in term of volume may be as

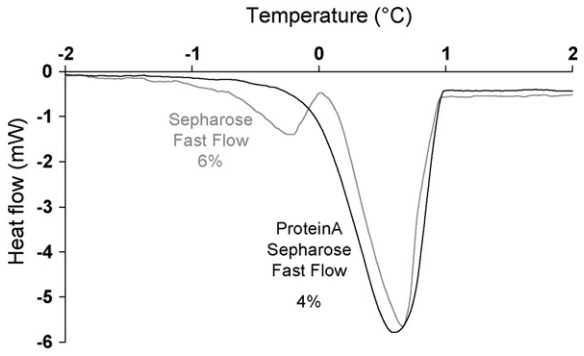

Fig. 12. DSC recordings for Sepharose SPFF and Protein A Sepharose.

high as 30% of the total pore volume and is not detected at all by ISEC.

The analysis of thermoporometry results shows two types of behaviour: independently of the pore size, as measured by ISEC, samples either give rise or do not give rise to a calorimetric peak corresponding to confined water. This is for example illustrated in Fig. 12 for SPFF and Protein A SPFF. The former material gives rise to a melting peak corresponding to confined water whereas the second one does not show it. It is noteworthy that the reticulation levels are 4 and 6%, respectively. Theoretically, this method should be well adapted to soft systems. Scherer et al. [25] showed that the constraint imposed by the freezing of water to the pore walls is by 10% lower than the one exerted by mercury. Nevertheless this constraint is still probably too large for some of the systems studied here. Surprisingly, one may observe that for the systems that does not give rise to a separated peak for melting the onset point is so close to 0 °C that water seems not to be affected by the presence of the pore walls. The behaviour is no more that of water in pores. Perhaps a good picture is that of a polymer solution in water.

It has been suggested in the literature [26] that after melting, water may migrate from a given pore to a larger pore where refreezing affects the shape of the heat flow/temperature recording, leading to a displacement of DSC peaks towards higher temperature. This phenomenon, which depends on the gel rigidity and the thickness of the pore walls, leads to an overestimation of the pore size or to an impossibility to measure it when the melting peak is shifted at a too high temperature. Hay et al. [26] suggest to increase the heating rate in order to limit the diffusion phenomenon of water. We effectively observed in some cases that the position of the peaks was influenced by the scanning rate and the thermal history of the sample. Unfortunately, because of the large pore size of most of the samples studied here, it is not possible to get both data at a high scanning temperature rate and at temperatures very close to that of bulk melting.

Looking now at the results obtained by water desorption, the following remarks can be made. In regard to pore size, the simultaneous de-swelling of polymer walls and emptying of capillary pores prevented to make a rigorous calculation of the pore size. This is why no value of the pore size is given in Table 4 in the case of soft materials. The shift of apparent pore size towards high values means that departure of water due to de-swelling of the structure occurs at high relative pressure values as already observed in the past [27]. For example, we followed the Fractogel bed thickness as a function of relative pressure with a camera and observed that at a relative pressure of 0.98, it was decreased by a factor of 2. Nevertheless, the sensitivity of water desorption method to the physical state of water allows the determination of inter- and intraparticle water amount directly from the steps observed on the desorption isotherm. Table 4 shows that the values obtained for the corresponding volumes are in a very good agreement with those obtained by batch size-exclusion or chromatography.

The sorption of water in a swelling polymer is due to two driving forces: the capillary condensation, which leads to pore filling, and the solvation of polymer chains, which is at the origin of the polymer volume increase in the presence of the solvent. This volume increase may be also enhanced by double layer formation if the polymer chains contain ionic groups. The swelling ratio depends not only on the interaction between solvent and polymer segments but also on the reticulation of the polymer chain. The theory of Flory-Rehner [28], gives a relationship that shows an increase of swelling ratio with a decrease of reticulation. Bradley et al. [29] showed that the higher the concentration of reticulating monomers during the synthesis the lower is the swelling ratio independently of temperature and pH conditions. The reticulation amount has also an effect on the rigidity of the polymer and on its temperature resistance. Okay [30] has shown that if a porous reticulated polymer is dried under its glass temperature, the structure is stable, whereas a drying at a higher temperature leads to collapse of the structure.

It seems possible to use water desorption curve in some cases to deduce the contribution of water volume due to swelling and that due to capillarity. This is illustrated in Figs. 13 and 14 where mercury porosimetry and water desorption isotherms are presented for Fractogel, Fractoprep and FractoAIMS. These three samples present various reticulation ratios, decreasing in the order Fractogel, FractoAIMS, Fractoprep (Merck, personal communication). Without knowing details on the structure at a molecular level, the analysis of gas adsorption and mercury intrusion curves allows to confirm the mechanical differences between these samples. When dried to be studied by gas adsorption, the behaviour is different between Fractogel and the two other samples. Adsorption level of nitrogen is too small to be quantitatively exploited. The drying has induced pore network collapse.

On the contrary, the pore sizes determined for Fractoprep and FractoAIMS before (by ISEC or thermoporometry), during (by water desorption) or after (by mercury porosimetry and gas adsorption) drying are equivalent by the different methods (Table 4). It means that the pore size is only slightly modified by the swelling. The results of mercury porosimetry show that FractoAIMS is partly collapsed by the intrusion of mercury as shown by the extrusion curve which does not return on the intrusion curve when pressure is decreased. This is also the case for Fractogel but the volume corresponding to the compression of pore network (above 50 MPa) is much smaller than the corresponding one of FractoAIMS. For Fractoprep, the amount of extruded mercury is much larger, thus confirming its better rigidity. The second intrusion–extrusion cycle confirms that the smallest pores of Fractoprep have not been destroyed and intrusion occurs at the same pressure.

The pore volumes obtained by the various methods are, of course, different. For example, the intraparticle pore volume of Fractoprep deduced from mercury porosimetry is 0.6 mL/g against 4.7 mL/g for water desorption. This difference is due to the partial structure collapse during intrusion and to the contribution of de-swelling to water desorption. The good agreement between the pore sizes shows that the pore size is not modified by the swelling. Looking more carefully at the water desorption results (Fig. 14), several domains are identified. The differential distribution may indeed be divided in two contributions: one narrow at small radii that could correspond to pore emptying (the mean value of this peak is in agreement with size-exclusion values) and the other very wide extending apparently from μm to nm that could correspond to the de-swelling of the materials (and does not correspond to a real size). It confirms that water sorbed by solvation forces is eliminated at higher pressure than capillary water.

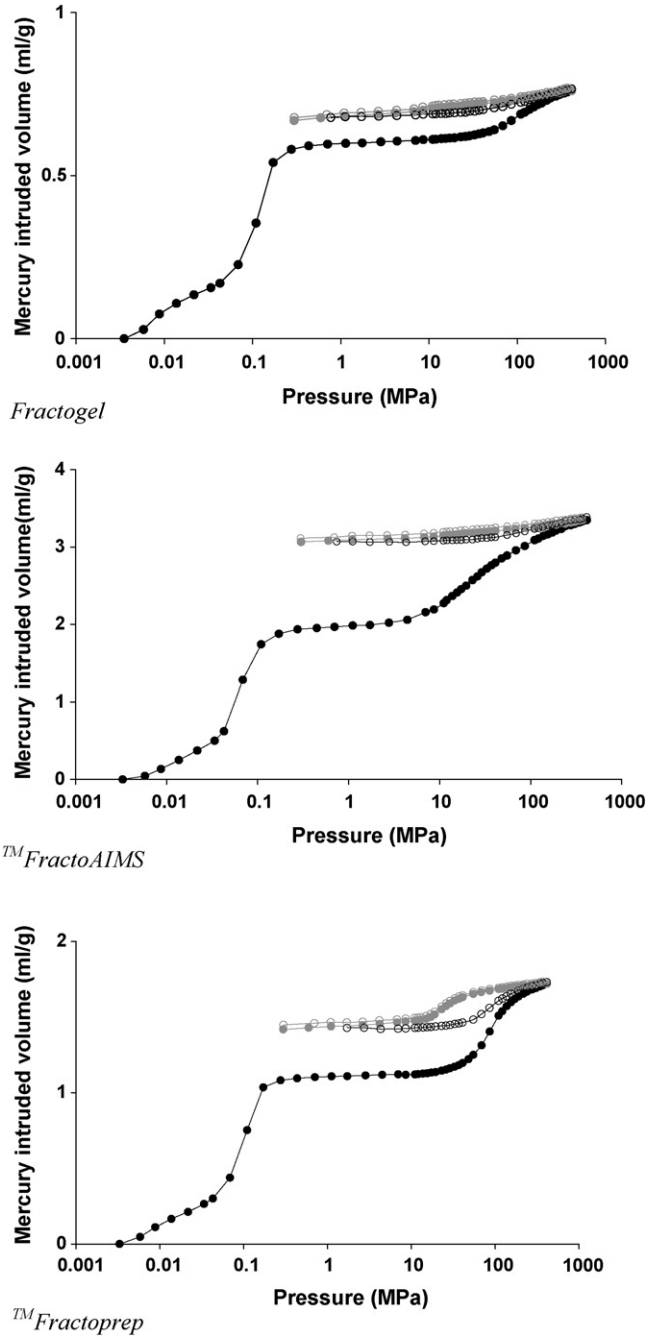

Fig. 13. Intrusion–extrusion of mercury on supports (2 cycles for each sample).

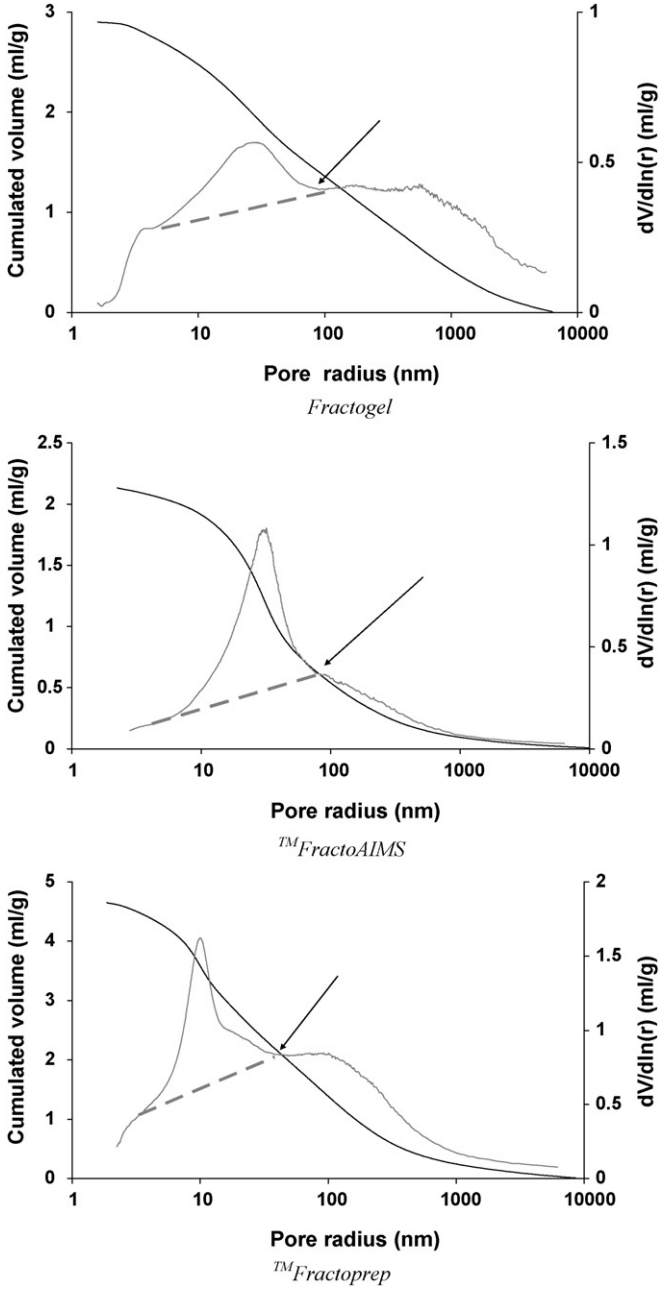

Fig. 14. Cumulative and differential pore size distribution obtained by water desorption for three supports. The arrows indicate the critical point at which the liquid–gas interface penetrates into the pores. The dotted line separates the contributions of volume filled by capillary phenomena and of swelling volume.

Smith et al. [31] explained that the de-swelling of a material starts as soon as the liquid–vapour interface reaches the particle pores, i.e. the interparticle volume is emptied. The diminution of pressure then produces a shrinking of polymer chains, which increases the mechanical strength of the materials. At a pressure called "critical drying pressure", the walls are strong enough to support the capillary pressure: the liquid–vapour interface may penetrate inside the pores that start to be emptied. The position of this critical point is indicated by an arrow in Fig. 14 for the three samples. If we consider that the peak delimited by a dotted line on these curves correspond mainly to pore filling (or emptying) by capillary condensation, then the area under this peak allows to calculate a pore volume whereas the difference between the total amount of water desorbed and the capillary water may give the amount of water participating to swelling. This allows calculating a swelling ratio by the following equation:

$$X_g = \frac{V_p + V_g + (1/d)}{V_p + (1/d)} \tag{19}$$

where V_p is the specific pore volume corresponding to capillary water, V_g is the specific volume of water involved in swelling and d is the density of the dried polymer. This swelling ratio is also calculated simply by measuring the bed thickness of the particles either in an excess of pure water and after drying in the same test tube. The results of the two types of measurement are given in Table 5, and show a very good agreement that reinforce the interpretation of water desorption data.

Table 5
Swelling ratio of support samples by two methods.

Method	Fractogel	™Fractoprep	FractoAIMS
Ratio of wetted and dried bed volume	3.3	3.1	1.6
Water desorption	3.2	3.2	1.7

4. Conclusions

When the rigidity of adsorbents is high enough, the agreement is reasonable between the values of the structural parameters that were determined (surface area, porosity, pore size) by the various methods. Nevertheless, a part of macroporosity may not be evidenced by inverse size-exclusion chromatography whereas it is determinable by batch exclusion and the other methods. When the rigidity decreases (as in the case of soft swelling gels) such that standard nitrogen adsorption or mercury porosimetry are no more reliable, two main situations are encountered: either the methods based on capillary phenomena overestimate the pore size with an amplitude that depends on the method, or in some cases it is possible to distinguish swelling water from capillary water. This swelling by water creates channels that are in the micropore range and exclude most of the probes used in size-exclusion measurements. Concerning the pore size range, the present study confirms or shows that (i) gas adsorption, as usually admitted, is applicable for pore sizes below 100 nm, (ii) inverse size-exclusion chromatography covers more or less the same range, excepted micropores, (iii) thermoporometry, provided low temperature scanning rates are used, is applicable from a few nm up to 300 nm, (iv) water desorption is applicable in the range 3 nm to 10 μm and (v) mercury porosimetry in its usual very large range from 3 nm to 300 μm.

Acknowledgement

This study was supported by a grant of the 6th Framework Program of EU, Project AIMs, No. NMP3-CT-2004-500160.

References

[1] F. Rouquerol, J. Rouquerol, K.S.W. Sing, Adsorption by Powders and Porous Solids, Academic Press, London, 1999.
[2] H. Giesche, Part. Part. Syst. Charact. 23 (2006) 9.
[3] N.A. Seaton, Chem. Eng. Sci. 46 (1991) 1895.
[4] P.J. Pomonis, K.M. Kolonia, G.S. Armatas, Langmuir 17 (2001) 8397.
[5] G.S. Armatas, C.E. Salmas, M. Louloudi, G.P. Androutsopoulos, P.J. Pomonis, Langmuir 19 (2003) 3128.
[6] I. Halasz, K. Martin, Ber. Bunsenges. Phys. Chem. 79 (1975) 731.
[7] Y. Yao, A.M. Lenhoff, J. Chromatogr. A 1037 (2004) 273.
[8] J. Hubbuch, T. Linden, E. Knieps, A. Ljunglof, J. Thommes, M.R. Kula, J. Chromatogr. A 1021 (2003) 93.
[9] M. Kremer, E. Pothmann, T. Rossler, J. Baker, A. Yee, H. Blanch, J.M. Prausnitz, Macromolecules 27 (1994) 2965.
[10] G. Grznarova, S. Yu, V. Stefuca, M. Polakovic, J. Chromatogr. A 1092 (2005) 107.
[11] I. Tatarova, M. Gramblicka, M. Antosova, M. Polakovic, J. Chromatogr. A 1193 (2008) 129.
[12] D. Lubda, W. Lindner, M. Quaglia, C. Du Fresne von Hohenesche, K.K. Unger, J. Chromatogr. A 1083 (2005) 14.
[13] B.A. Grimes, R. Skudas, K.K. Unger, D. Lubda, J. Chromatogr. A. 1144 (2007) 14.
[14] Z. Bayram-Hahn, B.A. Grimes, A.M. Lind, R. Skudas, K.K. K.K.Unger, A. Galarneau), J. Lapichella, F. Fajula, J. Sep. Sci. 30 (2007) 3089.
[15] M. Brun, A. Lallemand, J.F. Quinson, C. Eyraud, Thermochim. Acta 21 (1977) 59.
[16] I. Beurroies, R. Denoyel, P. Llewellyn, J. Rouquerol, Thermochim. Acta 421 (2004) 11.
[17] M. Pauthe, J.F. Quinson, J.D.F. Ramsay, Stud. Surf. Sci. Catal. 87 (1994) 283.
[18] M. Iza, S. Woerly, C. Danumah, S. Kaluiaguine, M. Bousmina, Polymer 41 (2000) 5885.
[19] R. Denoyel, M. Barrande, I. Beurroies, Stud. Surf. Sci. Catal. 160 (2007) 33.
[20] E.P. Barrett, L.G. Joyner, P.H. Hallenda, J. Am. Chem. Soc. 73 (1951) 373.
[21] G.D. Halsey, J. Chem. Phys. 16 (1948) 931.
[22] L. Hagel, M. Ostberg, T. Andersson, J. Chromatogr. A 743 (1996) 33.
[23] P. DePhillips, A.M. Lenhoff, J. Chromatogr. A 883 (2000) 39.
[24] J.C. Giddings, E. Kucera, C.P. Russell, M.N. Myers, J. Phys. Chem. 72 (1968) 4397.
[25] G.W. Scherer, D.M. Smith, D. Stein, J. Non-Cryst. Solids 186 (1995) 309.
[26] J.N. Hay, P. R. Laity 41 (2000) 6171.
[27] M.F. Refojo, ACS Symp. Ser. 44 (1976) 37.
[28] P.J. Flory, Principles of Polymer Chemistry, Ithaca and London Cornell University Press, 1953.
[29] M. Bradley, J. Ramos, B. Vincent, Langmuir 21 (2005) 1209.
[30] O. Okay, Prog. Polym. Sci. 25 (2000) 711.
[31] D.M. Smith, G.W. Scherer, J.M. Anderson, J. Non-Cryst. Solids 188 (1995) 191.